

NRCS-CN Estimation from Onsite and Remote Sensing Data for Management of a Reservoir in the Eastern Pyrenees

Marcos Sanz-Ramos¹; Belén Martí-Cardona, Ph.D.²; Ernest Bladé, Ph.D.³; Irene Seco, Ph.D.⁴; Arnau Amengual, Ph.D.⁵; Hélène Roux, Ph.D.⁶; and Romu Romero, Ph.D.⁷

Abstract: Onsite and Earth observation (EO) data are used for the calibration of the Natural Resources Conservation Service curve number (NRCS-CN) value in a hydrological simulation model. The model was developed for La Muga catchment (eastern Pyrenees) highly vulnerable to flood and drought episodes. It is an integral part of a regional reservoir management tool, which aims at minimizing the flood risk while maximizing the preservation of water storage. The CN values were optimized for five recorded events for the model to match the observed hydrographs at the reservoir when supported with the measured rainfall intensities. This study also investigates the possibilities of using antecedent moisture conditions (AMC) retrieved from satellite data to inform the selection of the NRCS-CN losses parameter. A good correlation was found between the calibrated CN values and the AMC obtained from satellite data. This correlation highlights the interest in using EO data to update NRCS-CN estimates. This advances in hydrologic-hydraulic coupled modeling combined with new remote sensing datasets present valuable opportunities and potential benefits for flood risk management and water resources preservation. DOI: [10.1061/\(ASCE\)HE.1943-5584.0001979](https://doi.org/10.1061/(ASCE)HE.1943-5584.0001979). © 2020 American Society of Civil Engineers.

Author keywords: Natural Resources Conservation Service curve number (NRCS-CN); Remote sensing; Flood risk; Reservoir management; Hydrological distributed modeling; Antecedent moisture condition (AMC); Mediterranean region.

Introduction

Droughts and floods are recurrent situations in Mediterranean catchments. In this semiarid region, streams are characterized by intermittent flows due to the irregularity of rainfall and the seasonal temperature variability. In a large portion of the Mediterranean region, highly urbanized areas and population seasonality due to tourism increase the water demands and at the same time the flood risk. Periods of water scarcity alternate with periods of frequent flooding that are becoming more severe under the influence of climate change (Arnell 1999; IPCC 2014b; Lehner et al. 2006).

The management of water resources in these water-stressed areas is therefore complex.

Floods are the most catastrophic natural hazard around the world (Fonseca et al. 2018; ISDR 2009; Kron 2005). In the Mediterranean region, according to the EM-DAT (2019) Disaster Database, floods are around 30% of the natural disasters that occurred in the twentieth century. On the other hand, droughts are a cyclic phenomenon in the Mediterranean region. Their management is a challenge for water administrations, especially during the summer season with its higher demand for water resources. The vulnerability of the Mediterranean area to droughts and floods is continually increasing due to the high economic dependency on water resources and the possible consequences of climate change (GECCC 2016; IPCC 2014a).

In this context, dams and reservoirs are essential elements for providing protection against flooding and ensuring the water supply year-round. The complexity of water resources and dam management requires the integration of several disciplines (meteorology, hydrology, and hydraulics, among others) and a deep knowledge of the system characteristics (catchment), inputs (rainfall), and outputs (demands). The use of realistic modeling that considers all these factors can lead to more effective predictions and more effective hazard mitigation.

At present, several modeling tools integrate two-dimensional hydraulic modeling with distributed hydrological modeling (Anees et al. 2017; Caro 2016; Cea et al. 2010; Kim et al. 2012; Roux et al. 2011; Viero et al. 2014; Yu and Duan 2017). Integrated or coupled modeling can better represent the real hydrologic and hydraulic processes than using these models independently. Nevertheless, models depend on a large number of parameters (e.g., soil and land characteristics and underground fluxes, among others) as well as on expertise in their implementation for risk and water resources management applications. The calibration and use of these tools can be complex because the number of the required parameters depends

¹Institut Flumen, Universitat Politècnica de Catalunya—International Center for Numerical Methods in Engineering, Barcelona 08034, Spain (corresponding author). ORCID: <https://orcid.org/0000-0003-2534-0039>. Email: marcos.sanz-ramos@upc.edu

²Dept. of Civil and Environmental Engineering, Univ. of Surrey, Guildford GU2 9PL, UK. Email: b.marti-cardona@surrey.ac.uk

³Institut Flumen, Universitat Politècnica de Catalunya—International Center for Numerical Methods in Engineering, Barcelona 08034, Spain. Email: ernest.blade@upc.edu

⁴Institut Flumen, Universitat Politècnica de Catalunya—International Center for Numerical Methods in Engineering, Barcelona 08034, Spain. ORCID: <https://orcid.org/0000-0003-0541-2605>. Email: irene.seco@upc.edu

⁵Grup de Meteorologia, Departament de Física, Universitat de les Illes Balears, Palma, Mallorca 07122, Spain. Email: arnau.amengual@uib.es

⁶Institut de Mécanique des Fluides de Toulouse, Université de Toulouse, CNRS, Toulouse 31400, France. Email: helene.roux@imft.fr

⁷Grup de Meteorologia, Departament de Física, Universitat de les Illes Balears, Palma, Mallorca 07122, Spain. Email: romu.romero@uib.es

Note. This manuscript was submitted on December 19, 2019; approved on April 17, 2020; published online on June 17, 2020. Discussion period open until November 17, 2020; separate discussions must be submitted for individual papers. This paper is part of the *Journal of Hydrologic Engineering*, © ASCE, ISSN 1084-0699.

often on limited data or on data with inadequate quality, and are not always directly physically measurable.

In this context, this paper first presents the results of the implementation and calibration of a coupled hydrological and hydraulic model. This model was used as a tool to define and implement management strategies for the Boadella Dam, located in the upper part of La Muga catchment (northeast of Spain). This model belongs to a series of methods developed under the Forecasting and Management of Flood Risk in the Pyrenees-Mediterranean Euroregion (PGRI-EPM) project for the operational management of reservoirs in the region (Roux et al. 2020; Sanz-Ramos et al. 2018). The designed management method is mainly based on modeling in a cascade of the involved processes (short-term precipitation forecast and coupled hydrologic and hydraulic processes). The objective is to minimize the flood risk and at the same time maximize the preservation of water resources during the management of extreme events.

The main factors that influence flood generation are related to the rainfall characteristics and the physical and hydrological characteristics of the catchment. The losses, mainly by infiltration and interception, are a determining factor in the rainfall-runoff transformation process. One of the most extended methods for losses estimation is the Soil Conservation Service curve number method (SCS-CN) (NRCS 2004), also referred to as the NRCS-CN method after the Soil Conservation Service was renamed the Natural Resources Conservation Service. The fact that it requires only one parameter for modeling losses has contributed to its success. In the NRCS-CN method, the curve number (CN) parameter, although not physically based, is a quantitative descriptor that embodies the complex physical characteristics of the soil type, antecedent soil moisture conditions (AMC), and land use and cover (LULC) in a catchment. Hence, a proper choice of the CN value is essential to achieve realistic rainfall-runoff simulations.

The determination of the AMC and thus of the CN value can be improved with the use of remote sensing techniques. These techniques provide spatially distributed retrievals for a wide variety of

hydrological parameters (Estévez et al. 2014; Martí-Cardona et al. 2013, 2010; Ramos-Fuertes et al. 2013; Torres-Batló et al. 2019; Wu et al. 2018), including surface soil moisture (SM). Also, remote sensing is a powerful tool for the observation of the hydrological processes and a relevant source of information for the calibration of numerical models describing such processes (Li et al. 2019; Ramos-Fuertes et al. 2013). The hydrological modeling community is progressively benefiting from the incorporation of spatial soil moisture measurements, with a varied degree of success (Brocca et al. 2017). Remote sensing has been used for indirect estimation of the CN value by obtaining land-use information from satellite images (Tirkey et al. 2014), but also for the adjustment of loss parameters (Silvestro et al. 2015). Rajib et al. (2016) explored the usage of spatially distributed remotely sensed soil moisture in the calibration of a hydrological model.

Against this background, this work aims at showing the relevance of remote-sensed soil moisture data for the CN estimation within a coupled distributed hydrologic-hydraulic model procedure oriented at water reservoir management. This main objective is achieved through three secondary goals applied on a case study: (1) set up and calibration of the hydrological model; (2) analysis of the variability of the CN within several registered events; and (3) identification of a relationship between the calibrated CN values and the estimated SM data from EO. The application of this technique in the study case is intended to provide better information for integrated flood risk and water resources management in continuous modeling.

Study Area

Site and Catchment Characteristics

La Muga is a cross-border basin of 961 km² located at the northeast of Catalonia (northeast Spain) that drains from the southeast Pyrenees to the Mediterranean Sea [Fig. 1(a)]. The basin is partially regulated by the Boadella Dam (182 km²), at the upper part of the

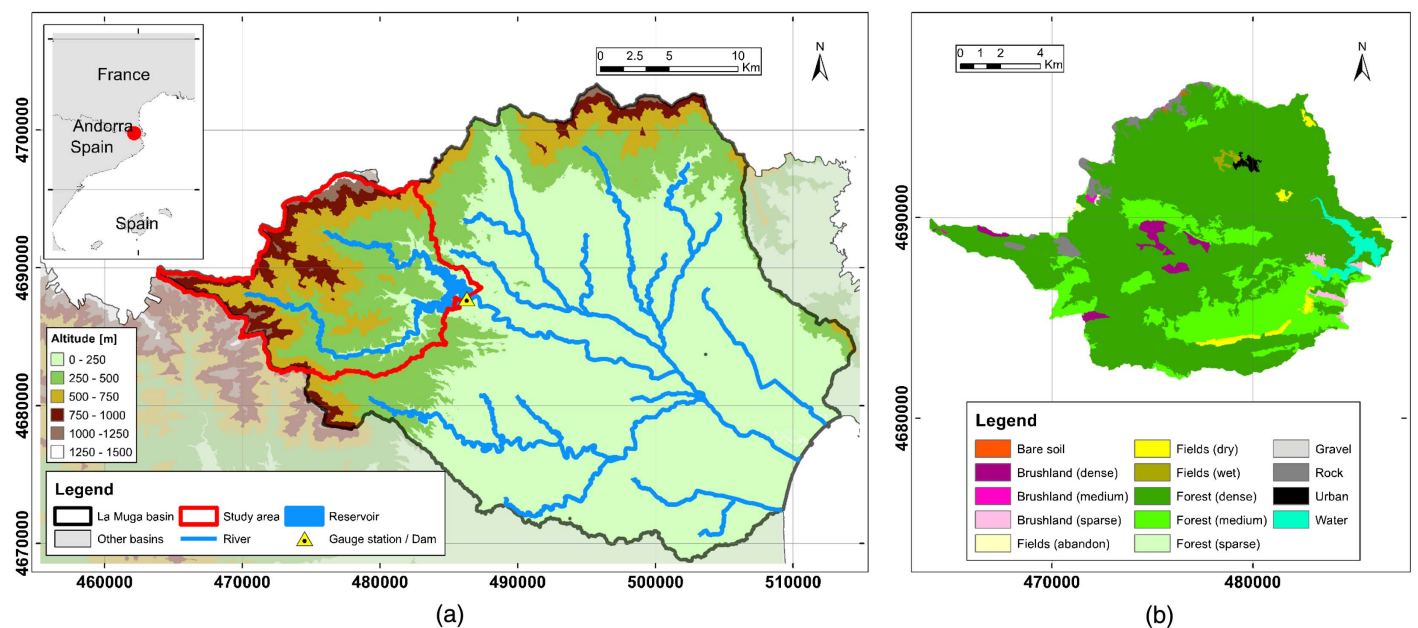


Fig. 1. Location and characteristics of the study area: (a) topography of La Muga Basin, extension of the study area, and location of the Boadella Dam and rain gauge station [reprinted from ICGC 2020, licensed under Creative Commons Attribution 4.0 International (CC-BY 4.0), <https://creativecommons.org/licenses/by/4.0/>]; and (b) land-use map of the study area (data from EEA 2007).

Table 1. Extreme rainfall events registered in the study area used for the model calibration

Event ID	Date	Season	Source of data	Total rainfall depth (mm)		Maximum intensity	
				<i>rg</i>	<i>r</i> ^a	Values per mm/5-min	Values per mm/h
20110313_4d	March 2011	Spring	<i>rg</i>	127	—	62	—
20130304_3d	March 2013	Spring	<i>rg</i>	181	—	30	—
20131116_3d	November 2013	Autumn	<i>rg, r</i>	123	98	54	9
20141129_2d	November 2014	Autumn	<i>rg, r</i>	151	132	61	13
20150320_3d	March 2015	Spring	<i>rg, r</i>	197	77	67	9

Note: *rg* = rain gauge; and *r* = for radar images for rainfall information sources.

^aCumulated rainfall for the study area.

^bIntensity registered in 5 min at the rain gauge.

^cIntensity registered in the study area.

catchment, with 62 hm³ of storage and a regulating capacity of 15 hm³. The basin, which includes some highly developed tourist areas at its lower part (Costa Brava), is highly vulnerable to drought due to excessive water demand (agriculture and human consumption) and flooding (ACA 2007).

The topography of the study area ranges from mountains to lowlands [Fig. 1(a)], and the rainfall regime in the catchment is significantly influenced by the Mediterranean Sea. The average annual rainfall ranges from 550 mm near the coast to 1,200 mm in the upper part. Heavy rainfall episodes tend to concentrate in late summer, autumn, and spring, lasting from several hours up to a few days. The variable rainfall frequency and long dry periods cause the area to suffer from severe water scarcity (Llasat and Rodriguez 1992; Martín-Vide 1994).

This work focuses on the upper part of La Muga basin, upstream of the Boadella Dam, where there is a single rainfall gauge and one water-level gauge [Fig. 1(a)]. The study area has an extension of 181 km² and is mainly characterized by large-forest coverage (above 90%) [Fig. 1(b)], low permeability, and low ground storage capacity (ACA 2007). The reservoir is included in the hydrological analysis and modeling, and it has been calibrated with the measures of water level and their variations during extreme rainfall events.

Data Set

Rainfall and Water Level

A detailed analysis of extreme rainfall events was performed within the PGRI-EPM project (Sanz-Ramos et al. 2018), through which more than 60 significant rainfall episodes registered during the last 100 years were evaluated. From the results of that analysis, five extreme rainfall events were selected for calibration of the proposed model (Table 1). The selected events, which occurred between

March 2011 and March 2015, are labeled with the starting date and the duration in days. The selected episodes have all mean rainfall intensities above 20 mm/h in 5 min and total precipitation volumes over 120 mm in periods between 2 and 4 days.

The data of precipitation and water level in the reservoir were provided by the Servei Meteorològic de Catalunya (SMC) and Agència Catalana de l'Aigua (ACA), respectively. They consisted of 5-min hyetographs recorded at the Boadella Dam station, rasters of 1 × 1 km spatially distributed hourly rainfall derived from radar (Bech et al. 2005; Corral et al. 2009), and the evolution of the water level in the reservoir (5-min resolution).

Digital Terrain Model and Land Uses

Topographical data were derived from a high-resolution 2 × 2 m digital terrain model (DTM) provided by the Institut Cartogràfic i Geològic de Catalunya (ICGC). The DTM includes the bathymetry of the reservoir above 145.0 meters above the sea level (m.a.s.l.) (below the minimum water level during the events).

Land-use data obtained from the CORINE project (EEA 2007) were used for the implementation of the surface roughness coefficient (*n* Manning coefficient). Additional details regarding these data can be found in Table 2.

Soil Moisture Data

Soil moisture data were obtained from the European Space Agency Climate Change Initiative for Soil Moisture (ESA CCI SM) (Liu et al. 2011, 2012; Wagner et al. 2012). The combined product version 4.2 (Chung et al. 2018) was obtained for the periods covering the selected rainfall events and for some days prior to their onset, with a maximum of 50 days. The product consists of daily rasters of volumetric soil moisture for the soil's top 20 mm. The rasters are provided with a spatial resolution of 0.25°, which for the study area corresponds to approximately 27.5 km.

Table 2. Summary of the data used for the upper La Muga subcatchment study case

Data type	Characteristics	Source	Data description
Digital terrain model	2 × 2 m ASCII raster file	Institut Cartogràfic i Geològic de Catalunya (ICGC 2020)	Elevation data based on light detection and ranging (LIDAR) (RMSE of 0.15 m)
Land uses	Shapefile converted into 2 × 2 m ASCII raster file	CORINE Land Cover project (EEA 2007)	Land uses classification and spatial representation for the year 2012
Soil moisture	0. 25°s patial resolution	European Space Agency Climate Change Initiative for Soil Moisture (ESA CCI SM)	ESA CCI SM
Precipitation	Rainfall intensities	Agència Catalana de l'Aigua (ACA) and Servei Meteorològic de Catalunya (SMC)	Rainfall intensities from 5-min rain gauge (hyetograph) and 1-h radar (1 × 1 km ASCII raster file)
Dam outlet/water level	Discharges and water level	Agència Catalana de l'Aigua (ACA)	5-min series of the outlet hydrograph and the water level in the reservoir

La Muga catchment is encompassed by two resolution cells of the ESA CCI SM product. In this case, 85 % of the catchment area overlays a raster cell entirely located on the southern Pyrenees, and the remaining 15 % falls within a cell mainly covering the northern Pyrenean side. Moisture data from both cells exhibit a markedly distinctive behavior, as expected from the different precipitation regimes on either side of the mountain range. Because the study catchment belongs to the southern Pyrenees, only the ESA CCI SM moisture records from the southern cell were used, assuming that they would better represent the catchment moisture status than a weighted average of both cells.

Methods

The cascade workflow presented herein is as follows: (1) building up a coupled hydrological-hydraulic numerical model balancing the computational cost and the results' accuracy; (2) calibrating the numerical model (CN and n) with onsite data, first with rain gauges and then fine-tuning with radar data; and (3) relating the CN values with EO data (SM) aiming to obtain the information needed to continuously support the numerical model for the reservoir management in future events.

Numerical Model

The coupled distributed hydrological and hydraulic numerical tool Iber (Bladé et al. 2014b; Cea and Bladé 2015) was used for both rainfall-runoff transformation and flow characterization. Iber is based on the dynamic wave solution of the shallow water equations (SWE) with the finite-volume method (Cea et al. 2016; Toro 2009), and it includes a specific numerical scheme for overland flow named decoupled hydrologic discretization (DHD) (Cea and Bladé 2015). After it was released in 2010, Iber has undergone several improvements. These enhancements allow the model to consider precipitation and losses varying in time and space and improved mesh definition for very shallow flows (i.e., a fill-sinks option) (Bladé et al. 2014a; Caro 2016; Cea et al. 2015; Cea and Bladé 2015; Juárez et al. 2014).

Additionally, Iber implements a specific drying method for hydrological computations, which handle the transition from wet to dry conditions, and vice versa. Briefly, a wet-dry limit (ε_{wd}) is used to define the water depth threshold below which a cell is considered to be dry. For drying cells, the scheme uses an

adaptation to finite-volume numerical schemes of the method used in LISFLOOD (Bates and De Roo 2000) in order to guarantee mass conservation. This method reduces numerical instabilities during simulation and ensures that all mesh cells have a zero or positive depth.

Model Setup

The study area was spatially discretized using an irregular triangular mesh of approximately 50,000 elements of area from 150 m² (in rivers) up to 200,000 m² (in hill slopes) (Fig. 2). This discretization is a compromise between accuracy of the results and computational time. The DTM was treated using a fill-sinks algorithm, based on the algorithm proposed by Wang and Liu (2006), to ensure a good definition of the flow path removing unreal depressions (Fig. 2). The DHD scheme was used with a wet-dry limit threshold of 10⁻⁴ m.

The current setup configuration allowed the simulation of events that last from 2 to 4 days with a computational time between 1 and 3 h using one CPU core (i7 fourth generation to 3.5 GHz). It is worth mentioning that since the end of the project, there have been substantial improvements in the computational time of Iber by using graphics processing unit (GPU) computing techniques (García-Feal et al. 2018). With this novelty, the presented simulations would run in about 1 min, achieving speed up of up to 100.

There is only one initial condition imposed to the model, which is the water level in the reservoir at the beginning of the simulation events. The river was assumed to be dry at the beginning of the simulations, which is an acceptable assumption because normal discharges are negligible when compared with flood discharges. No boundary conditions were imposed because there are no streams flowing into the study area. Rainfall intensities were applied on the corresponding mesh element. Manning coefficients (n) were associated with each element based on their land use according to the CORINE map (EEA 2007) [Fig. 1(b)].

The NRCS-CN method was used to evaluate the losses in the rainfall-runoff process. For its application, the initial abstraction (I_a) was linked to the soil potential retention (S) through a 0.2 factor ($I_a = 0.2 \cdot S$) as proposed by USDA (1986) and Ponce and Hawkins (1996). Due to the homogeneity of land uses, soil type, and AMC conditions in the study site, where over 90% of the area corresponds to forest coverage [Fig. 1(b)], a single value of CN was used for the whole basin. The value of CN was later adjusted within the calibration process.

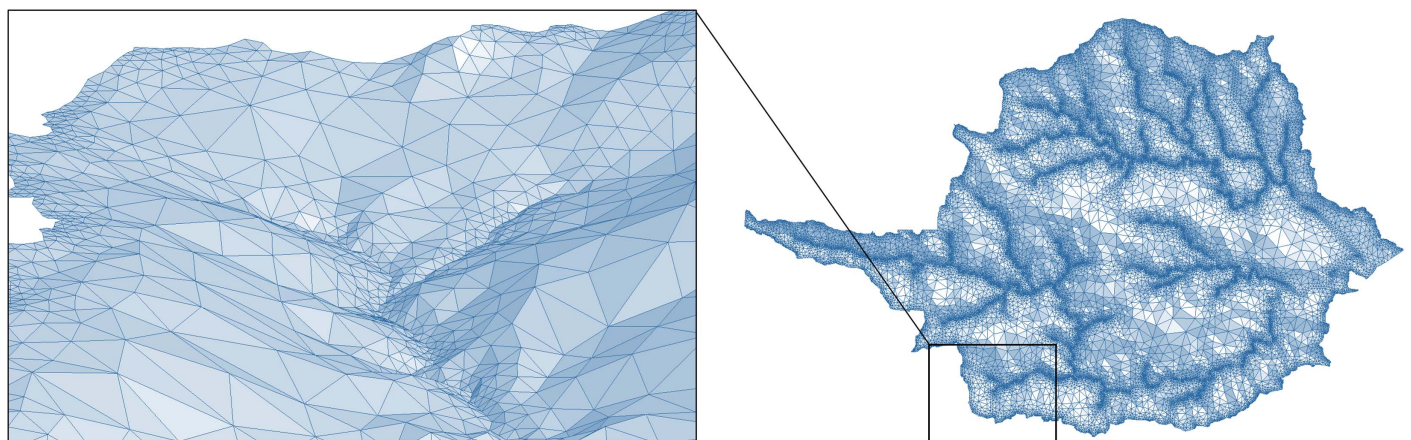


Fig. 2. Computational mesh of the study area.

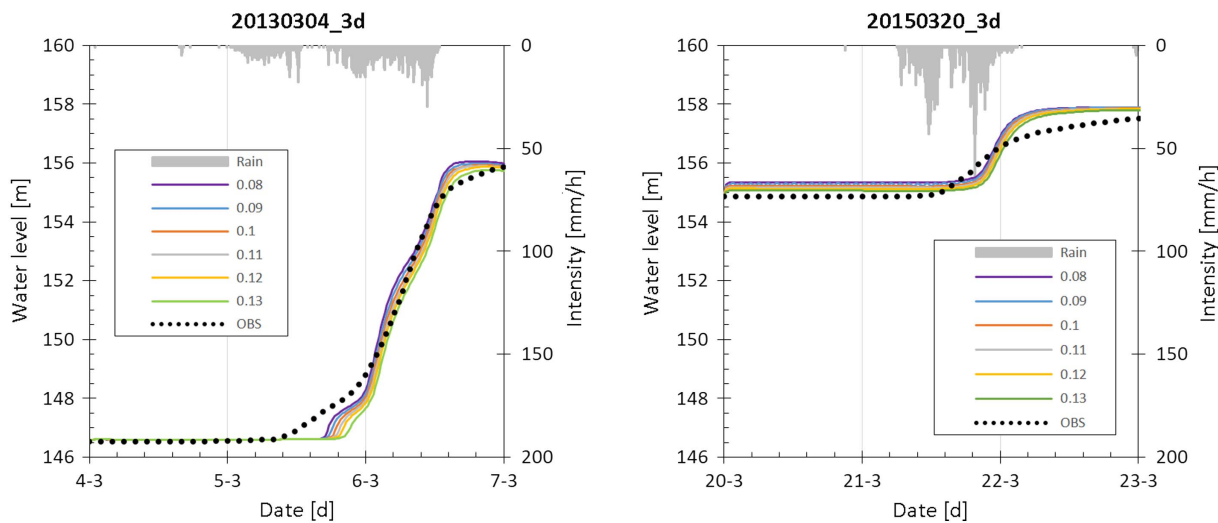


Fig. 3. Sensibility analysis for the Manning coefficient (n) associated with forest-dense land use: water-level evolution for the events 20130304_3d and 20150320_3d.

Relating CN to Earth Observation Soil Moisture Data

ESA CCI SM data provide information of the soil moisture in the top 20-mm layer of the soil. These measurements are well-correlated with previous rainfall days but might not be representative of the AMC, which have a relevant influence on the CN value. In this study, it was assumed that the evolution of daily surface moisture over several days before the onset of the rainfall event could inform of the water content in deeper soil layers, and hence it could be used as a proxy of the AMC and CN. In order to explore this relationship, daily SM values were averaged for periods ranging from 2 to 40 days before the beginning of the analyzed rainfall event. Then, a correlation between the averaged SM and the calibrated CN values was established.

Results and Discussion

Hydrological Modeling and Calibration Strategy

The purpose of the calibration process is the adjustment of the values of CN and the terrain roughness (n). The CN mainly influences on the mass balance of the whole event, whereas the n coefficient is expected to have an effect on the water front propagation and water elevation evolution.

A sensitivity analysis of the Manning's roughness coefficient was carried out. The reference values for the n coefficients were determined following the recommendations from the USGS guide (Arcement and Schneider 1989). A 0.11 value of n was assumed for the dense-forest land use that represents around 75% of the study area [Fig. 1(b)]. As a result of the analysis, no significant influence on the model response in terms of water front and water elevation in the reservoir was observed under n variations in a range of $\pm 20\%$. Hence, it is assumed that CN is the main calibration parameter. Results obtained by using the dense-forest land-use data for the n sensitivity analysis are shown in Fig. 3.

The CN was adjusted during calibration process to properly represent the evolution of the water stored in the reservoir during the events. For events 20110313_4d and 20130304_3d, rain data were available only from the rain gauge source. For events 20131116_3d, 20141129_2d, and 20150320_3d, data from both rain gauges and radar were available and used in the calibration

process. For these last three events, the gauge data are used for a first estimation of the CN value and what the authors called CN_{rg} . This value of CN was later fine-tuned with the radar information, calling it CN_r .

Table 3 indicates the CN value that best fit for all five events taking into account each data source. A seasonal trend could be inferred from these values, with higher values of CN during spring and moderate during autumn, although the number of events is not large enough to take more quantitative conclusions of seasonal variations.

In the study area, there are two alternative sources of information for the CN values: CEDEX (2003) and ACA (2019). Both are georeferenced databases available online and provide values of the initial abstraction from which the value of CN can be derived. According to CEDEX, the mean CN value for the study area is 64.9 ± 7.6 standard deviation, whereas according to ACA, it is 62.0 ± 12.8 under so-called normal catchment conditions (neither wet nor dry). If possible variations due to AMC are considered according to NRCS (2004), the CN values can be updated and varies in a range from 44.5 to 81.1 (initial CN from CEDEX database) and from 41.5 to 79.1 from ACA information. Thus, the CN values obtained from the calibration process for this study area and rainfall events are within the limits of values that would be obtained from these data provided by the public administration. However, the CN values provided by the mentioned public entities may be based on an outdated topographic base (Campón et al. 2015). Thus, the values that can be obtained by an ad hoc calibration using hydrological models and real rainfall data should generally provide more representative values of CN.

Table 4 presents the total cumulated rainfall and the effective rainfall for each event from rain gauge data and radar data. For the events

Table 3. CN values resulting from the calibration process

Event	Season	CN_{rg}	CN_r	$CN_{selected}$
20110313_4d	Spring	94	— ^a	94
20130304_3d	Spring	81	— ^a	81
20131116_3d	Autumn	50	55	55
20141129_2d	Autumn	60	65	65
20150320_3d	Spring	50	85	85

^aNo data available in this format.

Table 4. Cumulated and effective rainfall using the selected CN (Table 3) at the end of the event

Event	Total rainfall (mm)		Effective rainfall (mm)	
	rg	r	rg	r
20110313_4d	127	— ^a	109	— ^a
20130304_3d	181	— ^a	125	— ^a
20131116_3d	123	98.3	16	12
20141129_2d	151	132.3	59	49
20150320_3d	197	76.7	152	41

^aNo data available on this format.

20131116_3d, 20141129_2d, and 20150320_3d, with radar data set available, significant differences between the effective rainfall derived from gauge data and from radar were observed. The gauge station registered higher cumulative rainfall than values obtained from the radar source. Thus, in general, the estimated CN_{rg} is smaller than the CN_r in order to reach the same water level in the reservoir. For events 20131116_3d and 20141129_2d, the differences between this two CN values can be considered reasonable. However, for the event 20150320_3d, this difference is significant (Table 3). Regarding this, it can be hypothesized that there may have been a highly non-uniformly distributed rainfall. The gauge station probably registered high intensities locally concentrated around the gauge's location, which were not representative of the global rain pattern in the catchment during the event. This situation can be corroborated from radar data, which are analyzed subsequently.

The total rainfall cumulated at the end of the events 20131116_3d, 20141129_2d, and 20150320_3d is also represented in Fig. 4. The nonuniformity is easily observable in the rainfall spatial distribution recorded by the radar. For the event 20131116_3d, the maximum cumulated precipitation registered by the gauge (123 mm) is close to the radar maximum (120 mm). However, this value is observed only locally at the south of the study area, and the average rain depth is lower for the radar source than from the gauge source. For this reason, the CN_r is higher than the CN_{rg} . For the event 20141129_2d, the distribution of radar rainfall shows high

Table 5. Model performance between observed and simulated flow and water balance using the corresponding CN for each rain source

Event	MAE (m)		RMSE (m)		NSE	
	Gauge	Radar	Gauge	Radar	Gauge	Radar
20110313_4d	0.735	— ^a	0.873	— ^a	— ^b	— ^a
20130304_3d	0.261	— ^a	0.389	— ^a	0.987	— ^a
20131116_3d	0.193	0.152	0.209	0.172	0.637	0.754
20141129_2d	0.770	0.371	0.948	0.532	0.518	0.848
20150320_3d	0.383	0.242	0.432	0.260	0.861	0.941

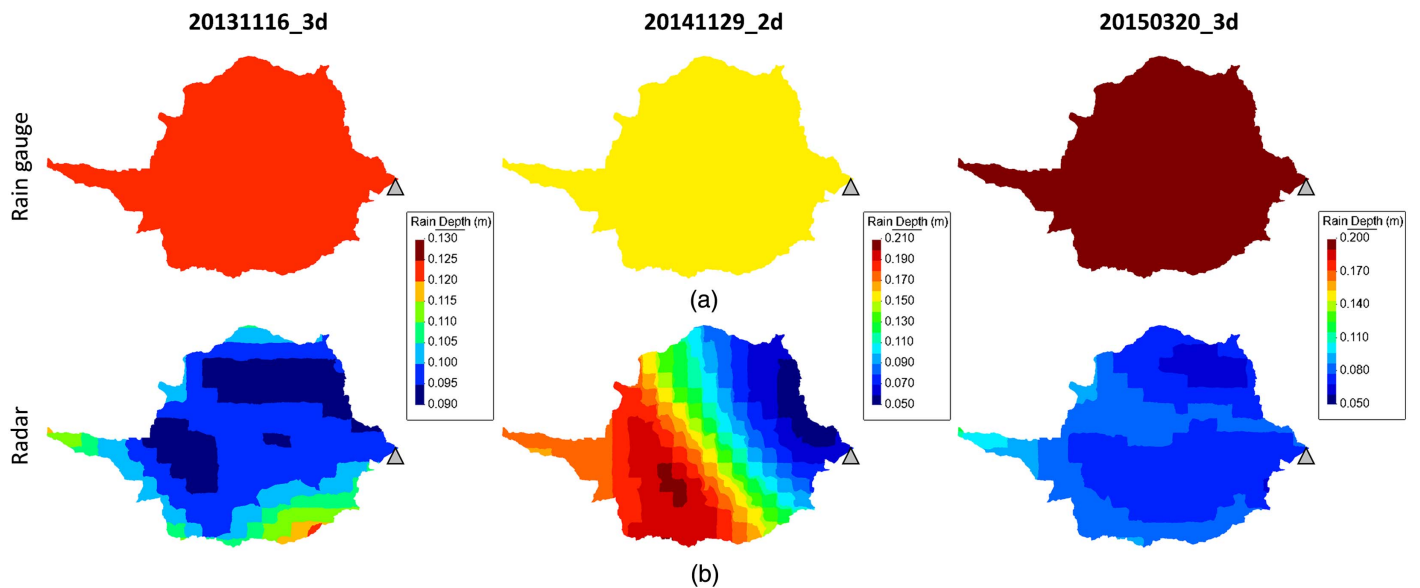
^aNo data available on this format.

^bStatistic not applicable due to lack of data.

accumulations at the east part of the study area (205 mm). However, the average values from gauge and radar are very similar (slightly higher for the rain gauge). Thus, the CN_r for this event is also slightly higher than CN_{rg} . Finally, for the event 20150320_3d, the differences are the largest. In this case, the cumulated rainfall from the rain gauge source is 200 mm whereas the radar does not exceed 80 mm (average value). As mentioned previously, a high local rainfall was registered by the rainfall station, which is not representative of the rainfall pattern in the basin, which in turn could explain the large differences between the CN_{rg} and the CN_r .

Based on what has been observed so far, the calibration process therefore focused on the adjustment of the CN value. The CNs finally selected by event indicated in Table 3 were a combination of the calibration process according to the best statistical fitting (Table 5). Thus, the CNs value derived from the calibration process ($CN_{selected}$) range between 55 and 94 (Table 3).

For the assessment of the fitting between observed and simulated results (water level at the dam) several indicators were used: mean absolute error (MAE), root-mean square error (RMSE), and Nash-Sutcliffe model efficiency coefficient (NSE) (Nash and Sutcliffe 1970). Table 5 summarizes the performance of the model for both rainfall data sources by event. In general, the simulations performed from radar (r) source data produce a better fit than those obtained with the gauge (rg) data in terms of water front evolution. This statement can be seen in Table 5 through the

**Fig. 4.** Representation of (a) nondistributed (triangle is the rain gauge localization); and (b) distributed rainfall records for events 20131116_3d, 20141129_2d, and 20150320_3d.

smallest mean differences (MAE and RMSE) and highest values of NSE.

Fig. 5 shows the performance of the model for both rain sources with the selected CN value. Events 20110313_4d and 20130304_3d, calibrated with rain gauge data, show in general a good performance. The modeled water level rise in the reservoir is slightly delayed with respect to the observed data, and the water level at the end of the event was slightly higher than the observed one. A slightly overestimation of the water level was observed at the end of events 20131116_3d and 20141129_2d. For the event 20150320_3d instead, the water level obtained from the rain gauge data rapidly increase exceeding the capacity of the reservoir (160 m.a.s.l.), far from the prediction made with radar data. Regarding the inconsistencies using gauge data in this last analyzed event, the authors refer to the nonuniform spatial distribution of the rainfall that may explain this result, as was previously explained.

It can be seen then that the availability of radar rainfall data can help to improve the hydrological model results because timely rainfall measurements provided by a rainfall station might be not enough representative of the complex spatial rainfall variation at the catchment scale. Moreover, rainfall data obtained from radar have a much higher spatial resolution (1 km² in this case), which allow a better spatial representation when modeling.

Tables 6 and 7 provide the results of the mass balance in the reservoir through the differences between observed data and simulation results for the gauge station and radar data, respectively. The differences in water level (WL_{start} and WL_{end}) and stored volume (V_{start} and V_{end}) at the start and end of the simulation period are shown for all the events. In general, good agreement between both observed and simulated results for the simulations performed with either data from the station or radar sources are observed. However, a significant difference is predicted for the event 20150320_3d. For this last event, a 252% difference in stored volume can be observed from the simulations carried out using gauge data. As previously hypothesized, significant differences observed using rain gauge data could be generated due to high localized rainfall near the gauge location.

For event 20110313_4d, the obtained CN value is close to the highest value of the parameter, which would imply that the losses are minimal. This unusually high value can be explained by two possible reasons: (1) the limitations of working with only one gauge, and (2) possible errors in the water-level records in the reservoir (the water evolution during the days before the event or the lack of data). With respect to the first cause suggested, from the Fig. 5 (Event 20110313_4d, dotted line) the water level in the reservoir increases during the first period although there is no rainfall registered by the gauge. This means that either it could have rained heavily during the previous days or there was rain in some parts of the basin that was not registered by the gauge. Additionally, some errors (lack of data and sudden steps) were detected on the water-level records registered in the reservoir. The initial water level was 151 m (constant value during the first 3 h of the simulation period), but after 10 min, it increased to 152 m. This difference means 2.67 hm³ in terms of water volume in the reservoir, which is around 12% of the volume stored during the event. These considerations are presented here as possible reasons that explain the high value for the CN calibrated for this episode.

On the other hand, the estimated CN for the event 20130304_3d is 81, also using rain gauge data. As shown in Fig. 5, the delay in the arrival time of the water front into the reservoir is approximately 10 h, but there is a good adjustment in terms of water levels after that. For the mentioned episode, the difference in water level in the reservoir at the end of the episode is lower than 0.03 m.

Relationship between Earth Observation–Based Soil Moisture Data and Curve Number

Fig. 6 illustrates the relationship between the five calibrated CNs and the daily EO surface moisture values averaged for different periods prior to the five rainfall events. For clarity, not all analyzed periods are represented in Fig. 6. As the number of averaged days approaches 16, the relationship between CN and averaged SM converges to a clear linear trend.

Fig. 7 depicts the squared linear correlation coefficient between CN and averaged surface moisture for all analyzed averaging periods and rainfall events. The best fit is achieved when 16 days prior to the rainfall onset are averaged, yielding a high R^2 value of 0.96. The clear consistency in the correlation coefficient changes as the antecedent period is varied reinforces the validity of this result.

The presented relationship between CN and EO based on surface moisture has been obtained for five rainfall events modeled in the small Boadella Reservoir catchment. Despite the limited representativeness of the presented case, the quality and consistency of the relationship strongly suggests the potential of EO data to provide updated estimates of the CN value. The accuracy in the estimation of this parameter has crucial implications in the volumes of runoff predicted by hydrological models, and, hence, in the flood prevention measures taken by water resources managers.

Discussion: Impact of Flooding and Potential Benefits of Merging Remote Sensing Data in Water Resources Management Decision Support Systems

Among the five events presented herein, the events 20110313_4d and 20130304_3d were the ones that caused more flood damages from an economic point of view. The economic evaluation of the flood risk associated to the released discharges, and of the water resources lost or preserved after the extreme rainfall episodes, are part of the outputs of the system developed under the PGRI-EPM project for the operational management of reservoirs in the region (Sanz-Ramos et al. 2018). The application of management measures obtained as outputs from the system for the aforementioned events would have significant benefits in minimizing the flood risk and maximizing the preservation of water resources. For 20110313_4d for instance, the damages to property would have been reduced by 15%, expected injury by 62%, and expected fatalities by 48%, and a volume of 0.9 hm³ of water released from the reservoir would have been preserved. These values represent a reduction of the episode impact of approximately 3.3 million Eur. For 20130304_3d, material damages would have been reduced by 28%, injury by 81%, expected fatalities by 58%, and 0.2 hm³ of preserved water volume. In this last case, the reduction of the impact would have been around 2.9 million Eur (Bladé et al. 2018).

EO data represent a valuable source of information for hydrologic purposes and for water resources management, in general, through mapping water resources and monitoring hydrological parameters. Remote sensing techniques contribute to management systems modeling by providing updated estimates of different parameters, which can significantly improve the efficiency of such models and their robustness for forecasting. In this case, attention is focused on the benefits that can be obtained in water management modeling through the updated assessment of the CN value after the consideration of remotely sensed soil moisture information as described in previous section.

Once the numerical model is calibrated, the final system is supported up with only two sets of data: quantitative precipitation forecasts and soil moisture from EO. The model is executed continuously, updating the inputs with the last available ESA CCI SM data and precipitation forecasts (Roux et al. 2020). Threshold alerts

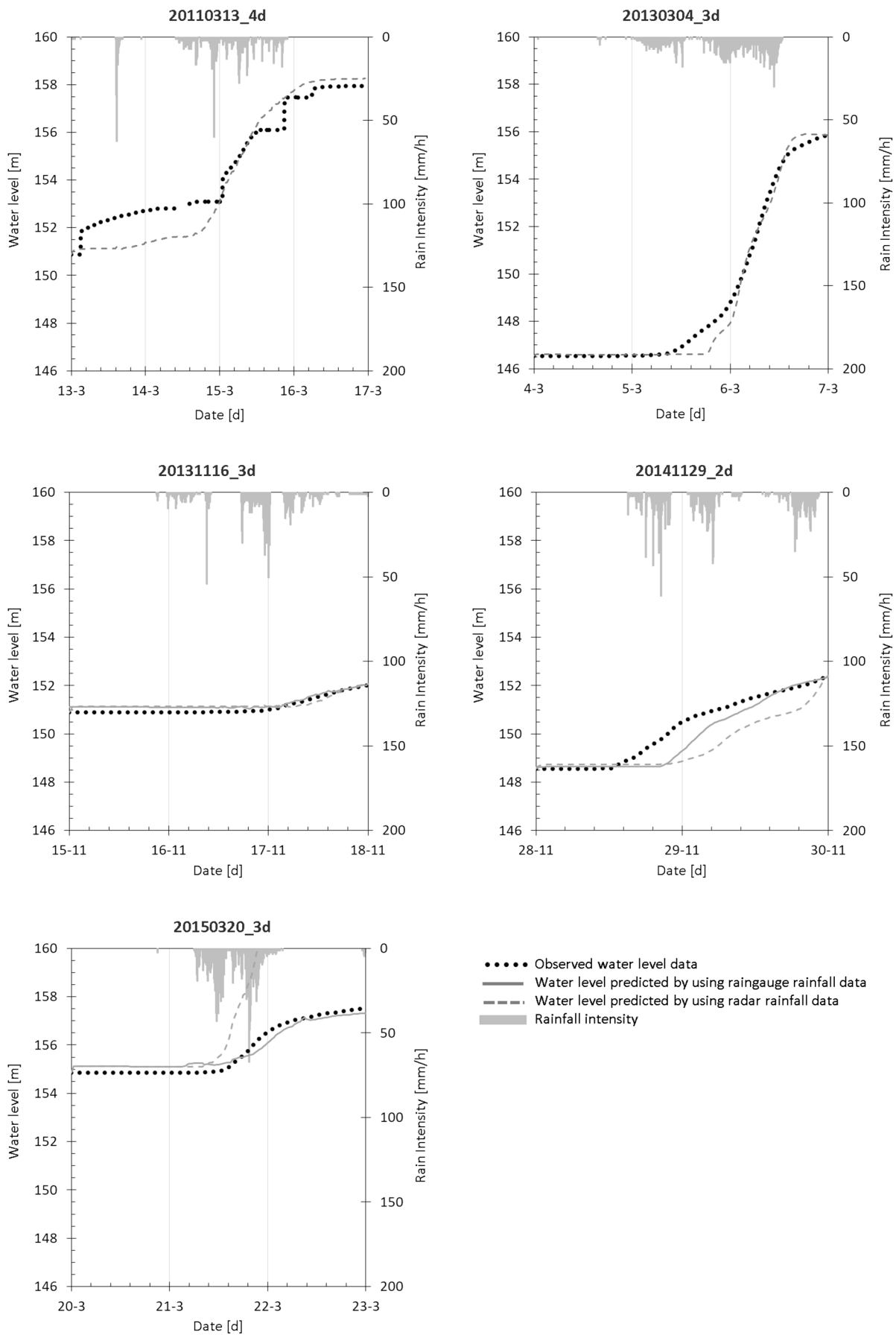


Fig. 5. Evolution of the water level in the Boadella Reservoir (dam point-check) for the observed data (dotted line) and simulations (rain gauge: dashed line and radar: continuous line) using the selected CN.

Table 6. Mass balance at the end of the rainfall event using gauge station data and the selected CN (Table 3)

Event	Gauge							
	WL _{start} (m)	WL _{end} (m)	V _{start} (hm ³)	V _{end} (hm ³)	ΔV (sim)	ΔV (obs)	Difference (hm ³)	Difference (%)
20110313_4d	151	158	36.9	60.2	23.3	22.2	1.1	4.9
20130304_3d	147	156	26.7	51.8	25.1	25.2	0.1	0.4
20131116_3d	151	152	37.0	40.2	3.23	3.07	0.16	5.2
20141129_2d	149	152	31.1	41.2	10.1	10.0	0.1	1.0
20150320_3d	155	163	48.5	80.2	31.7	9.0	22.7	252

Note: obs = observed; and sim = simulated.

Table 7. Mass balance at the end of the rainfall event using radar data and the selected CN (Table 3)

Event	Radar							
	WL _{start} (m)	WL _{end} (m)	V _{start} (hm ³)	V _{end} (hm ³)	ΔV (sim)	ΔV (obs)	Difference (hm ³)	Difference (%)
20131116_3d	151	152	37.0	40.2	3.23	3.07	0.16	5.2
20141129_2d	149	152	31.1	41.0	9.87	10.0	-0.14	-1.4
20150320_3d	155	157	48.5	56.8	8.24	8.95	-0.71	-7.9

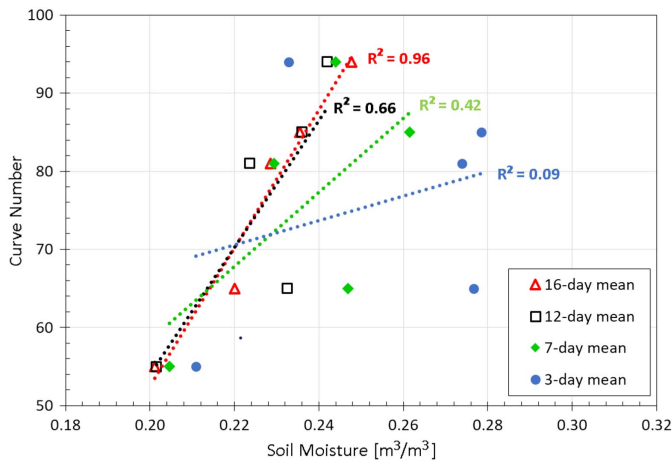


Fig. 6. Scatter plot of CNs calibrated for five events versus Earth observation-based soil moisture measurements averaged for different antecedent number of days.

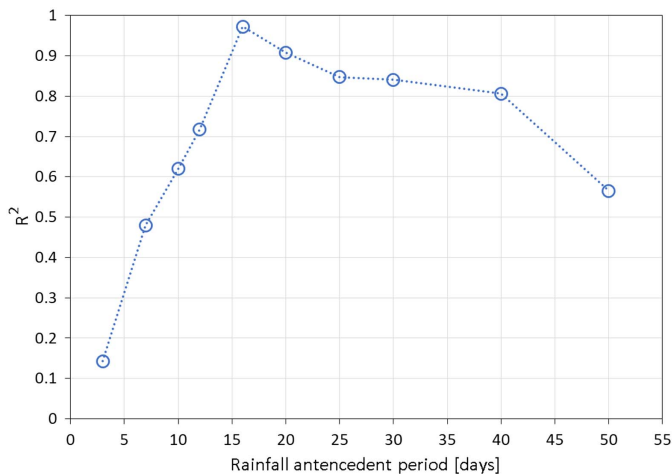


Fig. 7. R^2 coefficient of the linear correlation between the calibrated CNs and the Earth observation-based soil moisture averaged for different antecedent periods.

and pre-established dam operation protocols are included in the model, although the protocols can also be manually adjusted for the assessment of different operations of the dam outflow systems.

Conclusions

Onsite and EO data were used for the calibration of the NRCS-CN parameter of an eastern Pyrenees basin because it is the most important parameter of the hydrological model when correctly assessing water balance so as to evaluate the basin hydrologic response. The model developed for this purpose consists of a coupled fully distributed hydrological and hydraulic model, which constitutes the central core of an operational system for the Boadella Reservoir management. The main aim of the operational system is the prediction of flood risk and final water resources estimates associated to a forecasted extreme rainfall. The use of a distributed model integrating hydraulics and hydrology has been proven to be a robust tool so as to obtain in a single simulation, results of water resources (discharges and reservoir volumes), and flood hazard (depths and velocities).

Solid correlations were found between the estimated moisture data and the CN value obtained through numerical modeling forced by ground data, suggesting the potential of available remote sensing data for the updating of the CN values in continuous hydrological models. The optimal averaging period for the SM was, for the present case, 16 days. It would be valuable to check the validity of this period in other basins, which is proposed for future work.

The relationship between CN and EO based on surface moisture has been obtained for five rainfall events modeled in the small Boadella Reservoir catchment. The accuracy in the estimation of the CN parameter strongly affects the volumes of runoff simulated by the hydrological model and, consequently, the flood-mitigation measures informed by those.

Thanks to the SM-CN relationship, the information needed to continuously support the operational system for the reservoir management has been reduced to two sets of data: observed meteorological data in raster format, and the observed soil moisture. The consistency of the achieved SM-CN relationship strongly suggests the potential of EO data to provide updated estimates of the CN.

The present results of the application to the case study suggest the usefulness of incorporating remotely sensed proxies. This work is a step toward physical descriptors of soils based on remote

sensing and its integration in water resources management and flood forecasting systems, thus providing a beneficial direction for future work on optimized management strategies.

Data Availability Statement

The data used during the study, and provided by a third party are listed below:

- Precipitation data (Table 2), generated by Servei Meteorològic de Catalunya (<https://meteo.cat>), were provided by Agència Catalana de l'Aigua (<http://aca.gencat.cat/ca/inici>) within the PGRI-EPM project.
 - Dam outlet and water-level data (Table 2) were provided by Agència Catalana de l'Aigua (<http://aca.gencat.cat/ca/inici>) within the PGRI-EPM project.
- Direct requests for these materials may be made to the provider.

Acknowledgments

This work was carried out in the framework of the PGRI-EPM project (Prévision et gestion du risque d'inondation en Eurorégion Pyrénées Méditerranée) funded by the call for projects "Water Resources–Risk Management (Floods, Droughts, Submersion)" of the Pyrenees-Mediterranean Euroregion. The authors also thank to the Agència Catalana de l'Aigua and Servei Meteorològic de Catalunya, who provided the rainfall and water-level data, as well as its advisement during the project.

References

- ACA (Agència Catalana de l'Aigua). 2007. *Planificació de l'Espai Fluvial. Estudis d'inundabilitat en l'àmbit del projecte PEFCAT—Memòria específica Conca de La Muga*. Barcelona, Spain: ACA.
- ACA (Agència Catalana de l'Aigua). 2019. "Descàrrega cartogràfica." Accessed July 31, 2019. <http://aca.gencat.cat/ca/l'aigua/consulta-de-dades/descarrega-cartografica/>.
- Anees, M. T., K. Abdullah, M. N. M. Nordin, N. N. A. Rahman, M. I. Syakir, and M. O. A. Kadir. 2017. "One- and two-dimensional hydrological modelling and their uncertainties." In *Flood risk management*. London: InTech.
- Arcement, G. J. J., and V. R. Schneider. 1989. *Guide for selecting Manning's roughness coefficients for natural channels and flood plains*. USGS Water Supply Paper 2339. Washington, DC: USGS.
- Arnell, N. W. 1999. "The effect of climate change on hydrological regimes in Europe: A continental perspective." *Global Environ. Change* 9 (1): 5–23. [https://doi.org/10.1016/S0959-3780\(98\)00015-6](https://doi.org/10.1016/S0959-3780(98)00015-6).
- Bates, P., and A. P. De Roo. 2000. "A simple raster-based model for flood inundation simulation." *J. Hydrol.* 236 (1–2): 54–77. [https://doi.org/10.1016/S0022-1694\(00\)00278-X](https://doi.org/10.1016/S0022-1694(00)00278-X).
- Bech, J. T., N. Rigo, S. Pineda, E. Segalà, R. Vilaclara, R. Sánchez-Diezma, and D. Sempere-Torres. 2005. "Implementation of the EHIMI software package in the weather radar operational chain of the Catalan meteorological service." In *Proc., 11th Conf. on Mesoscale Processes and the 32nd Conf. on Radar Meteorology*. Boston: American Meteorological Society.
- Bladé, E., L. Cea, and G. Corestein. 2014a. "Numerical modelling of river inundations." *Ingeniería del agua* 18 (1): 68. <https://doi.org/10.4995/ia.2014.3144>.
- Bladé, E., L. Cea, G. Corestein, E. Escolano, J. Puertas, E. Vázquez-Cendón, J. Dolzand A. Coll. 2014b. "Iber: herramienta de simulación numérica del flujo en ríos." *Revista Internacional de Métodos Numéricos para Cálculo y Diseño en Ingeniería* 30 (1): 1–10. <https://doi.org/10.1016/j.rimmi.2012.07.004>.
- Bladé, E., M. Sanz-Ramos, A. Amengual, R. Romero, H. Roux, J. Savatier, and M. Cheriére. 2018. "Gestión integrada del riesgo de inundación y de los recursos hídricos empleando modelización integrada meteorológica, hidrológica e hidráulica." In *Proc., XI Jornadas Españolas de Presas*. Madrid, Spain: Comité Nacional Español de Grandes Presas.
- Brocca, L., W. T. Crow, L. Ciabatta, C. Massari, P. de Rosnay, M. Enenkel, S. Hahn, G. Amarnath, S. Camici, A. Tarpanelli, and W. Wagner. 2017. "A review of the applications of ASCAT soil moisture products." *IEEE J. Sel. Top. Appl. Earth Obs. Remote Sens.* 10 (5): 2285–2306. <https://doi.org/10.1109/JSTARS.2017.2651140>.
- Campón, L., E. Quirós, and P. Durán-Barroso. 2015. "Análisis de la variabilidad en la estimación del umbral de escorrentía en función de las distintas fuentes de información disponibles." In *Proc., IV Jornadas de Ingeniería del Agua*, 10. Córdoba, Spain: Universidad de Córdoba.
- Caro, C. A. 2016. "Modelación hidrológica distribuida basada en esquemas de volúmenes finitos." Ph.D. thesis, School of Civil Engineering, Universitat Politècnica de Catalunya.
- Cea, L., M. Bermúdez, J. Puertas, E. Bladé, G. Corestein, E. Escolano, A. Conde, B. Bockelmann-Evans, and R. Ahmadian. 2016. "IberWQ: New simulation tool for 2D water quality modelling in rivers and shallow estuaries." *J. Hydroinf.* 18 (5): 816–830. <https://doi.org/10.2166/hydro.2016.235>.
- Cea, L., and E. Bladé. 2015. "A simple and efficient unstructured finite volume scheme for solving the shallow water equations in overland flow applications." *Water Resour. Res.* 51 (7): 5464–5486. <https://doi.org/10.1002/2014WR016547>.
- Cea, L., I. Fraga, J. Puertas, M. Álvarez, M. Bermúdez, S. Coquerez, S. Salsón, and A. Pettazzi. 2015. "Influencia de la densidad espacial de estaciones pluviométricas y de la disponibilidad de datos radar en los hidrogramas de tormenta calculados con un modelo hidrológico distribuido: Aplicación a una cuenca de 24 km² en el Noroeste de España." In *Proc., Actas de las IV Jornadas de Ingeniería del Agua. Precipitación y procesos erosivos*. Córdoba, Spain: Universidad de Córdoba.
- Cea, L., M. Garrido, and J. Puertas. 2010. "Experimental validation of two-dimensional depth-averaged models for forecasting rainfall–runoff from precipitation data in urban areas." *J. Hydrol.* 382 (1–4): 88–102. <https://doi.org/10.1016/j.jhydrol.2009.12.020>.
- CEDEX (Centro de Estudios y Experimentación de Obras Públicas). 2003. *Análisis de nuevas fuentes de datos para la estimación del parámetro número de curva: Perfiles de suelos y teledetección*. Madrid, Spain: CEDEX.
- Chung, D., W. Dorigo, R. De Jeu, R. Kidd, and W. Wagner. 2018. *Product Specification Document (PSD) – D1.2.1 version 4.2*. Paris: European Space Agency.
- Corral, C., D. Velasco, D. Forcadell, D. Sempere-Torres, and E. Velasco. 2009. "Advances in radar-based flood warning systems. The EHIMI system and the experience in the Besòs flash-flood pilot basin." In Vol. 332 of *Proc., Flood Risk Management Research and Practice Extended Abstracts*, 1295–1303. Leiden, Netherlands: CRC Press.
- EEA (European Environmental Agency). 2007. *CORINE land cover 2006 technical guidelines*. EEA Technical Rep. No 17/2007. Copenhagen, Denmark: EEA.
- EM-DAT (Emergency Events Database). 2019. *Database | EM-DAT*. Brussels, Belgium: Université catholique de Louvain.
- Estévez, J., F. Moreno-Pérez, J. Roldán-Cañas, A. Serrat-Capdevila, J. González, F. Francés, F. Olivera, and J. V. Giráldez. 2014. "Hydrology and its role in water engineering." *Ingeniería del agua* 18 (1): 1. <https://doi.org/10.4995/ia.2014.3048>.
- Fonseca, A. R., M. Santos, and J. A. Santos. 2018. "Hydrological and flood hazard assessment using a coupled modelling approach for a mountainous catchment in Portugal." In *Stochastic environmental research and risk assessment*, 1. Berlin: Springer.
- García-Feal, O., J. González-Cao, M. Gómez-Gesteira, L. Cea, J. M. Domínguez, and A. Formella. 2018. "An accelerated tool for flood modelling based on Iber." *Water* 10 (10): 1459. <https://doi.org/10.3390/w10101459>.
- ICE (Institut d'Estudis Catalans). 2016. *Tercer informe sobre Canvi Climàtic a Catalunya*. Barcelona, Spain: ICE.
- ICGC (Institut Cartogràfic i Geològic de Catalunya). 2020. "Descàrregues." Accessed May 25, 2020. <https://www.icgc.cat/Descarregues>.

- IPCC (Intergovernmental Panel on Climate Change). 2014a. *Climate change 2013—The physical science basis*. Cambridge, UK: Cambridge University Press.
- IPCC (Intergovernmental Panel on Climate Change). 2014b. *Climate change 2014: Impacts, adaptation and vulnerability. Volume II: Global and sectoral aspects*. Geneva: IPCC.
- ISDR (International Strategy for Disaster Reduction) 2009. *Global assessment report on disaster risk reduction*. Geneva: United Nations.
- Juárez, D., J. Arganis, R. Dominguez, G. Esquivel, E. Bladé, J. Dolz, H. Sánchez-Tueros, and G. Corestein. 2014. "Comparación del hidrograma de salida de una cuenca con un modelo hidráulico y un modelo distribuido." In *Proc., XXIII Congreso Nacional de Hidráulica, Resúmenes extendidos*. Puerto Vallarta, Jalisco, México: Congreso Nacional de Hidráulica.
- Kim, J., A. Warnock, V. Y. Ivanov, and N. D. Katopodes. 2012. "Coupled modeling of hydrologic and hydrodynamic processes including overland and channel flow." *Adv. Water Resour.* 37 (Mar): 104–126. <https://doi.org/10.1016/j.advwatres.2011.11.009>.
- Kron, W. 2005. "Flood risk = Hazard + values + vulnerability." *Water Int.* 30 (1): 58–68. <https://doi.org/10.1080/02508060508691837>.
- Lehner, B., P. Döll, J. Alcamo, T. Henrichs, and F. Kaspar. 2006. "Estimating the impact of global change on flood and drought risks in Europe: A continental, integrated analysis." *Clim. Change* 75 (3): 273–299. <https://doi.org/10.1007/s10584-006-6338-4>.
- Li, H., D. Mao, X. Li, Z. Wang, and C. Wang. 2019. "Monitoring 40-year lake area changes of the Qaidam Basin, Tibetan Plateau, using Landsat time series." *Remote Sensing* 11 (3): 343. <https://doi.org/10.3390/rs11030343>.
- Liu, Y. Y., W. A. Dorigo, R. M. Parinussa, R. A. M. de Jeu, W. Wagner, M. F. McCabe, J. P. Evans, and A. I. J. M. van Dijk. 2012. "Trend-preserving blending of passive and active microwave soil moisture retrievals." *Remote Sens. Environ.* 123 (Aug): 280–297. <https://doi.org/10.1016/j.rse.2012.03.014>.
- Liu, Y. Y., R. M. Parinussa, W. A. Dorigo, R. A. M. De Jeu, W. Wagner, A. I. J. M. van Dijk, M. F. McCabe, and J. P. Evans. 2011. "Developing an improved soil moisture dataset by blending passive and active microwave satellite-based retrievals." *Hydrol. Earth Syst. Sci.* 15 (2): 425–436. <https://doi.org/10.5194/hess-15-425-2011>.
- Llasat, M. C., and R. Rodriguez. 1992. "Extreme rainfall events in Catalonia. The case of 12 November 1988." *Nat. Hazards* 5 (2): 133–151. <https://doi.org/10.1007/BF00127002>.
- Marti-Cardona, B., J. Dolz-Ripolles, and C. Lopez-Martinez. 2013. "Wetland inundation monitoring by the synergistic use of ENVISAT/ASAR imagery and ancillary spatial data." *Remote Sens. Environ.* 139 (Dec): 171–184. <https://doi.org/10.1016/j.rse.2013.07.028>.
- Martí-Cardona, B., C. Lopez-Martinez, J. Dolz-Ripolles, and E. Bladé. 2010. "ASAR polarimetric, multi-incidence angle and multitemporal characterization of Doñana wetlands for flood extent monitoring." *Remote Sens. Environ.* 114 (11): 2802–2815. <https://doi.org/10.1016/j.rse.2010.06.015>.
- Martín-Vide, J. 1994. "Geographical factors in the pluviometry of Mediterranean Spain: Drought and torrential rainfall." In *Proc., Spain Workshop on Natural Hazards*, 9–25. Iowa City, IA: Univ. of Iowa.
- Nash, J. E., and J. V. Sutcliffe. 1970. "River flow forecasting through conceptual models part I—A discussion of principles." *J. Hydrol.* 10 (3): 282–290. [https://doi.org/10.1016/0022-1694\(70\)90255-6](https://doi.org/10.1016/0022-1694(70)90255-6).
- NRCS (Natural Resources Conservation Service) 2004. "Part 630 hydrology—Chapter 10." In *National engineering handbook*, 79. Washington, DC: USDA.
- Ponce, V. M., and R. H. Hawkins. 1996. "Runoff curve number: Has it reached maturity?" *J. Hydrol. Eng.* 1 (1): 11–19. [https://doi.org/10.1061/\(ASCE\)1084-0699\(1996\)1:1\(11\)](https://doi.org/10.1061/(ASCE)1084-0699(1996)1:1(11)).
- Rajib, M. A., V. Merwade, and Z. Yu. 2016. "Multi-objective calibration of a hydrologic model using spatially distributed remotely sensed/in-situ soil moisture." *J. Hydrol.* 536 (May): 192–207. <https://doi.org/10.1016/j.jhydrol.2016.02.037>.
- Ramos-Fuertes, A., B. Martí-Cardona, E. Bladé, and J. Dolz. 2013. "Envisat/ASAR images for the calibration of wind drag action in the Doñana wetlands 2D hydrodynamic model." *Remote Sens.* 6 (1): 379–406. <https://doi.org/10.3390/rs6010379>.
- Roux, H., A. Amengual, R. Romero, E. Bladé, and M. Sanz-Ramos. 2020. "Evaluation of two hydrometeorological ensemble strategies for flash-flood forecasting over a catchment of the eastern Pyrenees." *Nat. Hazards Earth Syst. Sci.* 20 (2): 425–450. <https://doi.org/10.5194/nhess-20-425-2020>.
- Roux, H., D. Labat, P.-A. Garambois, M.-M. Maubourguet, J. Chorda, and D. Dartus. 2011. "A physically-based parsimonious hydrological model for flash floods in Mediterranean catchments." *Nat. Hazards Earth Syst. Sci.* 11 (9): 2567–2582. <https://doi.org/10.5194/nhess-11-2567-2011>.
- Sanz-Ramos, M., A. Amengual, E. Bladé, R. Romero, and H. Roux. 2018. "Flood forecasting using a coupled hydrological and hydraulic model (based on FVM) and high resolution meteorological model." In *Proc., E3S Web of Conf.* Les Ulis, France: EDP Sciences. <https://doi.org/10.1051/e3sconf/20184006028>.
- Silvestro, F., S. Gabellani, R. Rudari, F. Delogu, P. Laiolo, and G. Boni. 2015. "Uncertainty reduction and parameter estimation of a distributed hydrological model with ground and remote-sensing data." *Hydrol. Earth Syst. Sci.* 19 (4): 1727–1751. <https://doi.org/10.5194/hess-19-1727-2015>.
- Tirkey, A. S., A. C. Pandey, and M. S. Nathawat. 2014. "Use of high-resolution satellite data, GIS and NRCS-CN technique for the estimation of rainfall-induced run-off in small catchment of Jharkhand India." *Geocarto Int.* 29 (7): 778–791. <https://doi.org/10.1080/10106049.2013.841773>.
- Toro, E. F. 2009. *Riemann solvers and numerical methods for fluid dynamics*. Berlin: Springer.
- Torres-Batló, J., B. Martí-Cardona, and R. Pillco-Zolá. 2019. "Mapping evapotranspiration, vegetation and precipitation trends in the catchment of the shrinking Lake Poopó." *Remote Sens.* 12 (1): 73. <https://doi.org/10.3390/rs12010073>.
- USDA. 1986. *Urban hydrology for small watersheds*. Technical Release 55. Washington, DC: Natural Resources Conservation Service, Conservation Engineering Division.
- Viero, D. P., P. Peruzzo, L. Carniello, and A. Defina. 2014. "Integrated mathematical modeling of hydrological and hydrodynamic response to rainfall events in rural lowland catchments." *Water Resour. Res.* 50 (7): 5941–5957. <https://doi.org/10.1002/2013WR014293>.
- Wagner, W., W. Dorigo, R. A. M. de Jeu, D. Fernandez, J. Benveniste, E. Haas, and M. Ertl. 2012. "Fusion of active and passive microwave observations to create an essential climate variable data record on soil moisture." In *Proc., ISPRS Annals of the Photogrammetry, Remote Sensing and Spatial Information Sciences*, 315–321. Sydney, Australia: The Univ. of NSW. <https://doi.org/10.5194/isprannals-1-7-315-2012>.
- Wang, L., and H. Liu. 2006. "An efficient method for identifying and filling surface depressions in digital elevation models for hydrologic analysis and modelling." *Int. J. Geog. Inf. Sci.* 20 (2): 193–213. <https://doi.org/10.1080/13658810500433453>.
- Wu, Z., Z. Xu, F. Wang, H. He, J. Zhou, X. Wu, and Z. Liu. 2018. "Hydrologic evaluation of multi-source satellite precipitation products for the Upper Huaihe River Basin, China." *Remote Sens.* 10 (6): 840. <https://doi.org/10.3390/rs10060840>.
- Yu, C., and J. Duan. 2017. "Simulation of surface runoff using hydrodynamic model." *J. Hydrol. Eng.* 22 (6): 04017006. [https://doi.org/10.1061/\(ASCE\)HE.1943-5584.0001497](https://doi.org/10.1061/(ASCE)HE.1943-5584.0001497).